Insect Biochemistry and Molecular Biology 104 (2019) 82–90

Contents lists available at ScienceDirect

Insect Biochemistry and Molecular Biology

journal homepage: www.elsevier.com/locate/ibmb

Distinctive regulatory properties of pyruvate kinase 1 from *Aedes aegypti* mosquitoes

Natthida Petchampai[a], Claribel Murillo-Solano[a], Jun Isoe[b], Juan C. Pizarro[a,*], Patricia Y. Scaraffia[a,**]

[a] Department of Tropical Medicine, Vector-Borne Infectious Disease Research Center, School of Public Health and Tropical Medicine, Tulane University, New Orleans, LA, 70112, USA

[b] Department of Chemistry and Biochemistry, The University of Arizona, Tucson, AZ, 85721, USA

ARTICLE INFO

Keywords:
Crystal structure
Enzyme characterization
Glycolytic enzyme
Recombinant protein
Ammonia metabolism

ABSTRACT

Female *Aedes aegypti* mosquitoes are vectors of arboviruses that cause diseases of public health significance. The discovery of new metabolic targets is crucial for improving mosquito control strategies. We recently demonstrated that glucose oxidation supports ammonia detoxification in *A. aegypti*. Pyruvate kinase (PK, EC 2.7.1.40) catalyzes the last step of the glycolytic pathway. In most organisms, one or more allosteric effectors control PK activity. However, the kinetic properties and structure of PK in mosquitoes have not been previously reported. In this study, two alternatively spliced mRNA variants (AaPK1 and AaPK2) that code for PKs were identified in the *A. aegypti* genome. The AaPK1 mRNA variant, which encodes a 529 amino acid protein with an estimated molecular weight of ~57 kDa, was cloned. The protein was expressed in *Escherichia coli* and purified. The AaPK1 kinetic properties were identified. The recombinant protein was also crystallized and its 3D structure determined. We found that alanine, glutamine, proline, serine and fructose-1-phosphate displayed a classic allosteric activation on AaPK1. Ribulose-5-phosphate acted as an allosteric inhibitor of AaPK1 but its inhibitory effect was reversed by alanine, glutamine, proline and serine. Additionally, the allosteric activation of AaPK1 by amino acids was weakened by fructose-1,6-bisphosphate, whereas the allosteric activation of AaPK1 by alanine and serine was diminished by glucose-6-phosphate. The AaPK1 structure shows the presence of fructose-1,6-bisphosphate in the allosteric site. Together, our results reveal that specific amino acids and phosphorylated sugars tightly regulate conformational dynamics and catalytic changes of AaPK1. The distinctive AaPK1 allosteric properties support a complex role for this enzyme within mosquito metabolism.

1. Introduction

Glycolysis is a major metabolic pathway of glucose oxidation, providing energy and intermediate precursors for other pathways. Pyruvate kinase (PK, EC 2.7.1.40) catalyzes the irreversible transphosphorylation from phosphoenolpyruvate (PEP) and ADP to pyruvate and ATP (Kayne, 1973). The pyruvate product of PK plays a central role in cellular metabolism of both eukaryotes and prokaryotes as it feeds into a variety of metabolic pathways. PK requires both divalent (usually Mg^{2+} or Mn^{2+}) and monovalent (such as K^{+}) cations for its catalytic activity (Gupta et al., 1976; Kwan et al., 1975). In vertebrates, there are four different isoforms of PK, which are PKL, PKR, PKM1, and PKM2 (Hall and Cottam, 1978). The isoforms PKL, PKR, and PKM2 are allosterically regulated by fructose-1,6-bisphosphate (F16BP), whereas the PKM1 exhibits Michaelis-Menten kinetics (Hall and Cottam, 1978). Although F16BP is a major allosteric activator of PK, other sugars, such as fructose-2,6-bisphosphate (F26BP), glucose-6-phosphate (G6P), and ribose-5-phosphate, have been shown to regulate PK activity (Bakszt et al., 2010; Callens et al., 1991; Waygood et al., 1975).

The regulation of PK is important for controlling glycolytic flux, which sequentially impacts the levels of intracellular metabolite pools (Mattevi et al., 1996). In insects, PK from the flight muscles of American

Abbreviations: AaPK, *Aedes aegypti* pyruvate kinase; F1P, fructose-1-phosphate; F6P, fructose-6-phosphate; F16BP, fructose-1,6-bisphosphate; F26BP, fructose-2,6-bisphosphate; G6P, glucose-6-phosphate; LB, Luria-Bertani; PE, pentaerythritol ethoxylate; PMSF, phenylmethanesulfonyl fluoride; PEP, phosphoenolpyruvate; PEG, polyethylene glycol; PEG MME, polyethylene glycol monomethyl ether; PK, pyruvate kinase; PPP, pentose phosphate pathway; R5P, ribulose-5-phosphate; R15BP, ribulose-1,5-bisphosphate; TB, Terrific broth; TEA, triethanolamine

* Corresponding author.
** Corresponding author.
E-mail addresses: jpizarro@tulane.edu (J.C. Pizarro), pscaraff@tulane.edu (P.Y. Scaraffia).

https://doi.org/10.1016/j.ibmb.2018.12.010
Received 26 November 2018; Received in revised form 17 December 2018; Accepted 17 December 2018
Available online 19 December 2018
0965-1748/

cockroaches (*Periplaneta americana*) and desert locusts (*Schistocerca gregaria*) displayed Michaelis-Menten kinetics, whereas the enzyme from the fat body of the same organisms showed allosteric sigmoidal properties (Bailey and Walker, 1969; Storey, 1985). In mealworm beetles (*Tenebrio molitor*), the change in PK kinetic properties was observed during physiological alteration, such as injury, starvation, and insecticide or acetone injection (Papadopoulos, 2005). In *Aedes aegypti* mosquitoes, the primary vector of dengue, chikungunya, yellow fever and Zika viruses (Katzelnick et al., 2017; Monath and Vasconcelos, 2015; Wilder-Smith et al., 2017; Yun and Lee, 2017), PK activity was shown to be elevated throughout embryogenesis, suggesting an increase of glycolysis in *A. aegypti* embryos (Vital et al., 2010).

A. aegypti mosquitoes preferentially feed on human blood, and usually fly a short distance to ensure they stay in close proximity to human hosts (Harrington et al., 2001, 2005; Russell et al., 2005). In addition to carbohydrate sources, *A. aegypti* can use the amino acid proline to fuel flight via the proline-alanine cycle (Scaraffia and Wells, 2003). In this cycle, proline serves as a shuttle to move acetyl units between fat body and flight muscles. The pyruvate generated from different reactions, including decarboxylation of malate (Scaraffia and Wells, 2003) or as a product of PK can be utilized as a substrate of alanine aminotransferase, an enzyme involved in amino acid and ammonia metabolism in *A. aegypti* (Horvath et al., 2018; Isoe et al., 2017; Mazzalupo et al., 2016).

The metabolic requirements of female mosquitoes fluctuate throughout their lives, and the regulation of PK could be critical for particular metabolic needs, such as flight, starvation, sugar and blood meal digestion, waste disposal, reproduction and survival. In this report we biochemically and structurally characterized *A. aegypti* PK1 (AaPK1) *in vitro* to elucidate the factors that regulate the enzyme. We found that specific amino acids and phosphorylated sugars tightly regulate conformational dynamics and catalytic changes of AaPK1. The unique AaPK1 allosteric properties support a complex role for this enzyme within mosquito metabolism.

2. Materials and methods

2.1. Reagents

All primers and oligo-$(dT)_{20}$ were obtained from IDT (Coralville, IA, USA). Reverse transcriptase and GoTaq® DNA Polymerase were purchased from Promega (Madison, WI, USA). TRIzol® reagent, ampicillin, chloramphenicol, glycerol, CHAPS, imidazole, Pierce™ Universal Nuclease for Cell Lysis, HisPur™ Ni-NTA Resin, Pierce™ Microplate BCA Protein Assay Kit - Reducing Agent Compatible, PureLink™ Quick Plasmid Miniprep Kit, S.O.C. medium, and Luria-Bertani (LB) agar were acquired from Thermo Fisher Scientific Inc. (Waltham, MA, USA). Terrific broth (TB) was obtained from Gentrox (Worcester, MA, USA). *Escherichia coli* host strain NovaBlue and Rosetta-2, and pET-51b(+) Ek/LIC vector were purchased from EMD Millipore (Billerica, MA, USA). Index HT™ and PEG/Ion HT™ crystallization screens, 50% w/v polyethylene glycol (PEG) 3350, 100% polyethylene glycol monomethyl ether (PEG MME) 550, 50% v/v pentaerythritol ethoxylate (15/4 EO/OH) (PE) were acquired from Hampton Research Corp. (Aliso Viejo, CA, USA). Triethanolamine (TEA), PEP, ammonium citrate tribasic, L-lactic dehydrogenase from rabbit muscle, fructose-6-phosphate (F6P), F16BP, F26BP, G6P, ribulose-5-phosphate (R5P), ribulose-1,5-bisphosphate (R15BP), alanine, glutamine, glutamic acid, phenylalanine, proline, and serine were acquired from Sigma-Aldrich (St. Louis, MO, USA). Fructose-1-phosphate (F1P) was purchased from Santa Cruz Biotechnology, Inc. (Dallas, TX, USA). Isopropyl β-D-1-thiogalactopyranoside (IPTG), phenylmethanesulfonyl fluoride (PMSF), benzamidine, lysozyme, and HEPES were obtained from Fisher Scientific, Inc. (Hampton, NH, USA).

2.2. Insects, cloning, expression, and purification of AaPK1

The *A. aegypti* (NIH Rockefeller strain) colony was maintained at 28 °C, 75% relative humidity with a light: dark cycle of 16 h: 8 h as previously described (Isoe and Scaraffia, 2013). Total RNA was extracted from larva, pupa and adult *A. aegypti* using TRIzol reagent according to the manufacturer's protocol. First strand cDNA was synthesized from pools of total RNA using oligo-$(dT)_{20}$ primer and reverse transcriptase. Primers (AaPK1Fw gacgacgacaagATGATGGTCTGGGTGT CCGA and AaPK1Rv gaggagaagcccggTTCGACATTCACAATGCGAA TGG), that are specific to open reading frame (ORF) of AaPK1 with sequence extension for cloning into pET-51b(+) Ek/LIC vector, were designed based on AaPK1 mRNA variant sequence on Genbank (NCBI Reference Sequence: XM_001649933.1). ORF of AaPK1 was amplified from the mosquito cDNA using GoTaq® G2 Hot Start Green Master Mix with a final primer concentration of 100 nM. PCR conditions consisted of a 98 °C pre-incubation step for 2 min and 30 amplification cycles of 98 °C for 10 s, 55 °C for 1 min, and 72 °C for 1 min followed by a 5-min extension step at 72 °C. PCR product was cloned into pET-51b(+) Ek/LIC vector and transformed into NovaBlue *E. coli* according to the manufacturer's manual. The plasmids were isolated using PureLink Quick Plasmid Miniprep kit as described in the manufacturer's instructions. The identity of the inserts was confirmed by DNA sequencing (GENEWIZ, Inc., South Plainfield, NJ, USA).

The AaPK1 expression plasmid construct was transformed into Rosetta-2 *E. coli* as previously described (Bakszt et al., 2010). Briefly, after incubation on ice for 5 min and heat shocking at 42 °C for 30 s, 800 µl of S.O.C. medium was added and the cell suspension was incubated at 37 °C with shaking for 1 h. The cells were then collected by centrifugation at 900 × *g* for 5 min at 4 °C and the pellet was resuspended in 150 µl of S.O.C medium. Aliquots of 70 and 40 µl of the cell suspension were spread over the surface of LB agar plates supplemented with ampicillin and chloramphenicol (50 and 33 µg/ml, respectively) and incubated at 37 °C overnight. A single colony from the transformation was then inoculated into 25 ml of TB medium containing antibiotics (ampicillin and chloramphenicol at 50 and 33 µg/ml, respectively) and incubated at 37 °C with shaking overnight. Subsequently, the culture was transferred into 1 L of TB medium supplemented with antibiotics. The bacteria were grown at 37 °C until an OD_{600} reached 0.8–1.0 and then induced with 0.5 mM IPTG overnight at 25 °C. Cells were harvested by centrifugation at 4500 × *g* for 20 min at 4 °C. The pellet was then resuspended in 35 ml of binding buffer (50 mM HEPES pH 7.5, 500 mM KCl, 5 mM imidazole, 5% glycerol) supplemented with 1 mM PMSF and 1 mM benzamidine and stored at 80 °C until used. Resuspended cells were added with 0.5% CHAPS, 500 U of endonuclease, 0.5 mM PMSF and 0.5 mM benzamidine then incubated at room temperature with rotation. After 1 h, the lysate was centrifuged at 4500 × *g* for 20 min at 4 °C. The supernatant was then loaded onto a column pre-packed with 1 ml HisPur™ Ni-NTA Resin, pre-equilibrated with 10 ml double distilled water, at 1 ml/min. The column was washed with 100 ml wash buffer (50 mM HEPES pH 7.5, 500 mM KCl, 30 mM imidazole, 5% glycerol) at 3 ml/min. The protein was eluted with 14 ml elution buffer (50 mM HEPES pH 7.5, 500 mM KCl, 250 mM imidazole, 5% glycerol) and concentrated to a volume of about 2 ml using a filter with a molecular weight exclusion of 10 kDa (Amicon® Ultra-4 Centrifugal Filter Units, EMD Millipore). The final purification of the protein was performed with BioLogic Duo-Flow system (Bio-Rad, Hercules, CA, USA). A size-exclusion column pre-packed with Superdex 200 26/60 (GE Healthcare, NJ, USA) was pre-equilibrated in eluent (10 mM HEPES pH 7.5, 500 mM KCl) at a flow rate of 1 ml/min. Chromatography was performed at 4 °C and the protein was monitored for absorbance at 280 nm. Fractions (2 ml each) eluting at 25–32 min were collected, pooled, and concentrated to a volume of about 0.5–1 ml. The purified enzyme (Fig. S1) was used for enzymatic characterization and crystallography.

2.3. Crystallization and structure determination of recombinant AaPK1

Purified AaPK1 was crystallized using the sitting drop vapor diffusion method in which 1 μL of protein (16 mg/ml) was mixed with 1 μL crystallization reagent and 1 μL ligands (100 mM KCl, 5 mM ATP, 5 mM oxaloacetate, 1 mM F16BP) in a cyclic olefin copolymer protein crystallography plate (Corning Inc, Corning, NY, USA). Initial crystallization conditions were screened using Index HT™ and PEG/Ion HT™ crystallization screen (Hampton Research Corp.). Indext HT™ conditions E7 (0.05 M $MgCl_2$, 0.1 M HEPES pH 7.5, 30% v/v PEG MME 550), E9 (0.05 M ammonium sulfate, 0.05 M BIS-TRIS pH 6.5, 30% v/v PE), H4 (0.2 M ammonium citrate tribasic pH 7, 20% w/v PEG 3350) and H8 (0.1 M magnesium formate dehydrate, 15% w/v PEG 3350) and PEG/Ion HT™ condition F10 (0.2 M ammonium citrate tribasic pH 7, 20% w/v PEG 3350) were optimized by varying the salt and precipitant concentrations. Crystals were flash-frozen in liquid nitrogen with mother liquor solution containing 20% ethylene glycol as a cryoprotectant. Diffraction data for AaPK1 was collected at CAMD (Center for Advanced Microstructures and Devices, LSU, Baton Rouge, LA, USA) protein crystallography beamline. Data were processed and scaled using XDS package (Kabsch, 2014). The protein structure was determined by molecular replacement using the monomer PKM1 from rabbit PK (PDB id 3N25) as the search model and the Phaser (McCoy et al., 2007). To avoid model bias in the AaPK1 multimeric arrangement each monomer was searched independently by the molecular replacement procedure. Model building was performed in COOT (Emsley and Cowtan, 2004), and refinement and model validation were done using Phenix (Adams et al., 2010). The allosteric ligand F16BP was not included in the molecular replacement search model, nor was it included during the initial model. F16BP was included in the later refinement, and its presence was corroborated by simulated annealing OMIT maps as implemented in Phenix (Adams et al., 2010) (Fig. S2). Crystallographic coordinates were deposited in the Protein Data Bank (PDB id 6DU6).

2.4. PK activity assays and kinetic studies

PK activity was determined by following the changes of absorbance at 340 nm in a Synergy HT microplate reader (BioTek, Winooski, VT, USA) at 25 °C as previously described (Bakszt et al., 2010). The reactions were initiated by the addition of enzyme (diluted to yield a linear reaction for 5 min) to the following assay mixture: 50 mM TEA pH 7.5, 50 mM KCl, 20 mM MgCl2, 2 mM ADP, 0.2 mM NADH, 2 U L-lactic dehydrogenase, and 1 mM PEP. The concentration of the purified enzyme stock solution was 15 mg/ml. The assays were carried out immediately after the enzyme was diluted. Controls were performed in all the determinations by omitting the enzyme in the mixture. The molar extinction coefficient of 6.22 cm^2/μmol at 340 nm was used to calculate NADH oxidation. One unit of the enzyme is the amount that utilizes 1 μmol of substrate per minute under the assay conditions.

The kinetic parameters for PEP were determined by varying its concentration (0.0003, 0.0008, 0.0023, 0.0069, 0.0206, 0.0617, 0.1852, 0.5556, 1.6667, and 5 mM) under the above-mentioned reaction conditions with ~0.5 μg/ml of recombinant AaPK1. The affinity of the enzyme for PEP by several effectors including sugars (F1P, F6P, F16BP, F26BP, G6P, R5P, R15BP), and amino acids (alanine, glutamic acid, glutamine, phenylalanine, proline, and serine) was determined at 1 mM of each compound (Bakszt et al., 2010; Chan and Sim, 2004; Iliffe-Lee and McClarty, 2002). Reactions were carried out at 25 °C and were monitored for 3 min. Kinetic parameters were calculated from Allosteric-sigmoidal after a nonlinear curve-fitting of experimentally determined data, using GraphPad Prism version 6.0 for Mac OS X (GraphPad Software, San Diego, CA, USA). The curves were generated by using the equation $v = V_{max} * [S]^h/(K_{prime} + [S]^h)$, where v is enzyme velocity, V_{max} is the maximum enzyme velocity, [S] is substrate concentration, h is Hill coefficient, and K_{prime} is the concentration of substrate that produces a half-maximal enzyme velocity (Copeland, 2000).

2.5. Fluorescence thermal shift assays

The assays were performed in a 96-well plate (Axygen, Corning, NY, USA) with an assay volume of 20 μl. Purified AaPK1, each effector (sugars, amino acids or a combination of amino acids and sugars) and Sypro Orange (Invitrogen, Carlsbad, CA, USA) were diluted to 0.125 μg/μl (2.17 μM), 500 μM, and 5x, respectively, in a buffer containing 50 mM TEA pH 7.5, 50 mM KCl and 20 mM $MgCl_2$. The mixtures were aliquoted in triplicate into a 96-well plate, sealed with optical clear plastic seal, and centrifuged. Thermal scanning (18–90 °C at 1 °C/min) coupled with fluorescence detection was conducted using a real-time PCR machine (Bio-Rad CFX96 Touch Real Time system, Bio-Rad). Data were analyzed using DMAN software (Wang et al., 2012).

2.6. Statistical analysis

Statistical analyses were conducted using GraphPad Prism version 6.0 for Mac OS X (GraphPad Software). An unpaired Student's *t*-test was used to determine the effect of each individual sugar or amino acid, compared to the control, on AaPK1 activity. One-way analysis of variance (ANOVA) followed by Tukey's multiple comparison test was utilized to examine the influence of the sugar in combination with the amino acid. Data are presented as means of at least three independent samples. P values of ≤ 0.05 were considered significantly different.

3. Results

BLAST searches were performed at the National Center for Biotechnology and Information (NCBI) using *Drosophila melanogaster* PK sequence (accession number O62619) as the query for identifying PK genes in mosquitoes. Using AaegL5 genome assembly and AaegL5.1 geneset (Matthews et al., 2018), we determined that two alternatively spliced mRNA variants encoding PKs of 529 (AAEL014913) and 519 (AAEL012576) amino acid residues are located at single locus in the *A. aegypti* genome. *Culex quinquefasciatus* (CPIJ008289), *Anopheles gambiae* (AGAP004596) and *D. melanogaster* also have a single copy of PK in their respective genomes. *A. aegypti* PK shares 92%, 91% and 75% identity at the amino acid level in *Culex quinquefasciatus*, *Anopheles gambiae* and *D. melanogaster*, respectively.

We cloned and overexpressed AaPK1 as a recombinant protein in *E. coli*. The size of the purified protein corresponded to an estimated molecular weight analysis of a full-length cDNA sequence, which is about 57 kDa (Fig. S1). The AaPK1 enzyme was found to be active and the kinetic parameters were determined for substrate PEP, with the apparent K_{prime}, V_{max}, and h of 0.246 ± 0.021 mM PEP, 0.100 ± 0.001 mM NADH/min, and 1.08 ± 0.04, respectively (Table 1).

3.1. F1P activates AaPK1 by increasing the affinity of the enzyme to PEP

Although PK is controlled in many organisms by the allosteric effector F16BP, other sugars such as F1P, F26BP and G6P have been shown to regulate the activity of the enzyme (Bakszt et al., 2010; Callens et al., 1991; Eggleston and Woods, 1970; Mattevi et al., 1996; Van Schaftingen et al., 1985). Therefore, PK assays were carried out to evaluate the effect of various phosphorylated sugars (both five- and six-carbon) on AaPK1 kinetic parameters (Table 1 and Fig. 1A). The bi-phosphorylated sugars, F26BP and R15BP had no effect on the V_{max}. However, R5P increased the V_{max} by 31%, whereas F1P, F6P, F16BP, and G6P decreased the V_{max} by 21, 39, 32, and 48%, respectively. Among the sugars, F6P, F16BP, F26BP, G6P, and R15BP showed no effect on the K_{prime}. While F1P increased the affinity of AaPK1 to PEP with a 4-fold reduction in the K_{prime}, R5P decreased the affinity of the enzyme to the substrate with a 5-fold induction in the K_{prime}. Although,

Table 1
Effect of phosphorylated sugars and amino acids on AaPK1 kinetic parameters.

Effector	K_{prime} (mM PEP)	V_{max} (mM NADH/min)	*h*
Control	0.246 ± 0.021	0.100 ± 0.001	1.08 ± 0.04
Sugars			
F1P	0.057 ± 0.023[a]	0.079 ± 0.002	1.35 ± 0.15
F6P	0.193 ± 0.054	0.061 ± 0.003	0.80 ± 0.08
F16BP	0.386 ± 0.116	0.068 ± 0.005	0.70 ± 0.08
F26BP	0.088 ± 0.024	0.106 ± 0.003	1.46 ± 0.13
G6P	0.136 ± 0.054	0.052 ± 0.003	0.85 ± 0.11
R5P	1.130 ± 0.251[a]	0.131 ± 0.013	0.60 ± 0.05
R15BP	0.359 ± 0.067	0.102 ± 0.004	0.63 ± 0.04
Amino acids			
Alanine	0.044 ± 0.011[a]	0.087 ± 0.002	1.68 ± 0.11
Glutamic acid	0.175 ± 0.017	0.095 ± 0.001	1.34 ± 0.05
Glutamine	0.052 ± 0.028[a]	0.103 ± 0.004	1.34 ± 0.20
Phenylalanine	0.095 ± 0.019	0.095 ± 0.002	1.17 ± 0.08
Proline	0.022 ± 0.009[a]	0.102 ± 0.002	1.64 ± 0.16
Serine	0.072 ± 0.020[a]	0.094 ± 0.002	1.48 ± 0.13
Alanine and sugars			
Alanine/R5P	0.049 ± 0.014[a,b]	0.097 ± 0.002	1.34 ± 0.10
Alanine/F16BP	0.530 ± 0.119[a,c]	0.113 ± 0.008	0.62 ± 0.05
Alanine/G6P	0.361 ± 0.113[c]	0.104 ± 0.008	0.63 ± 0.07
Proline and sugars			
Proline/R5P	0.051 ± 0.012[b]	0.102 ± 0.002	1.50 ± 0.10
Proline/F16BP	0.537 ± 0.111[a,d]	0.120 ± 0.008	0.54 ± 0.04
Proline/G6P	0.219 ± 0.071	0.101 ± 0.006	0.72 ± 0.08
Glutamine and sugars			
Glutamine/R5P	0.595 ± 0.200[a,b,e]	0.102 ± 0.012	0.48 ± 0.06
Glutamine/F16BP	0.913 ± 0.225[a,e,f]	0.116 ± 0.012	0.51 ± 0.04
Glutamine/G6P	0.146 ± 0.050	0.077 ± 0.003	0.82 ± 0.09
Serine and sugars			
Serine/R5P	0.210 ± 0.048[b]	0.083 ± 0.003	0.93 ± 0.08
Serine/F16BP	1.076 ± 0.228[a,f,g]	0.112 ± 0.012	0.50 ± 0.04
Serine/G6P	1.065 ± 0.308[a,g,h]	0.110 ± 0.015	0.50 ± 0.05

AaPK1 = *Aedes aegypti* pyruvate kinase 1, F1P = fructose-1-phosphate, F6P = fructose-6-phosphate, F16BP = fructose-1,6-bisphosphate, F26BP = fructose-2,6-bisphosphate, G6P = glucose-6-phosphate, *h* = Hill coefficient, PEP = phosphoenolpyruvate, R5P = ribulose-5-phosphate, R15BP = ribulose-1,5-bisphosphate, [a] $P < 0.05$ when compared to control, [b] $P < 0.05$ when compared to R5P, [c] $P < 0.05$ when compared to alanine, [d] $P < 0.05$ when compared to proline, [e] $P < 0.05$ when compared to glutamine, [f] $P < 0.05$ when compared to F16BP, [g] $P < 0.05$ when compared to serine, [h] $P < 0.05$ when compared to G6P. Data points represent means ± SEM of at least three replicates.

most phosphorylated sugars reduced PEP binding cooperativity, F1P and F26BP showed positive cooperativity behavior. Therefore, our results indicate that F1P is an allosteric activator, while R5P is an allosteric inhibitor of AaPK1.

3.2. Alanine, glutamine, proline, and serine exhibit a classic allosteric activation on AaPK1

Three ligand-binding sites, including active site, effector site, and amino acid binding site, have been identified in PK in various organisms such as mammals, trypanosomatids, yeast, and bacteria (Chaneton et al., 2012; Collins et al., 1995; Fothergill-Gillmore et al., 2000; Lovell et al., 1998; Morgan et al., 2010; Suzuki et al., 2008). Thus, the effect of several amino acids on enzymatic activity of AaPK1 was examined (Table 1 and Fig. 1B). All amino acids tested including alanine, glutamic acid, glutamine, phenylalanine, proline, and serine exhibited cooperative binding of PEP with a characteristic sigmoid binding curve. Our data indicate that AaPK1 is regulated by alanine, glutamine, proline, and serine in a classic allosteric fashion with a reduction in the K_{prime} (4–13 fold) and no effect on the V_{max}.

3.3. Alanine, glutamine, proline, and serine prevent the inhibitory effect of R5P on AaPK1 activity

Next, we determined the effect of sugar and amino acid combinations on the AaPK1 kinetic parameters. Specifically, alanine, glutamine, proline, and serine (the four amino acids that dramatically increased the affinity of the enzyme to the substrate) were analyzed in combination with R5P (Table 1, Figs. 2 and 3). Interestingly, when the enzymatic assays were performed in the presence of alanine and R5P, the K_{prime} value was comparable to that observed in the presence of alanine alone (Table 1 and Fig. 2A). Likewise, a similar result was obtained when alanine was replaced by proline in the same assays (Table 1 and Fig. 2B): 5-fold reduction in the K_{prime} when compared to R5P alone. Additionally, the combination of these amino acids (alanine or proline) and the sugar R5P had no effect on the V_{max} and exhibited positive cooperativity for PEP when compared to the control. Although the addition of glutamine to the assay reactions containing R5P did not reduce the K_{prime} to that observed in the control or glutamine alone, the presence of glutamine in the reactions significantly decreased the K_{prime} (2-fold) when compared to R5P alone (Table 1 and Fig. 3A). A similar result was observed when glutamine was replaced with serine: 5-fold reduction in K_{prime} when compared to R5P alone (Table 1 and Fig. 3B). Furthermore, the addition of glutamine or serine to the reactions containing R5P showed no effect on the V_{max} and weakened positive cooperativity for PEP binding. These results indicate that alanine, proline, glutamine and serine prevent the *in vitro* inhibition of AaPK1 activity caused by R5P.

3.4. F16BP diminishes the effect of alanine, glutamine, proline, and serine on AaPK1 activity

Although F16BP alone had no effect on AaPK1, this sugar is a major allosteric activator of PK in several organisms. Thus, the effect of F16BP in combination with a selected amino acid (alanine, glutamine, proline, or serine) on AaPK1 activity was assessed. As shown in Table 1, Figs. 2 and 3, the addition of F16BP to the PK assay reactions containing each amino acid significantly increased the K_{prime} (2- to 4-fold) when compared to the control. Likewise, when compared to alanine, glutamine, proline, or serine alone, the combination of F16BP and each respective amino acid significantly increased the K_{prime} value of AaPK1 (13- to 27-

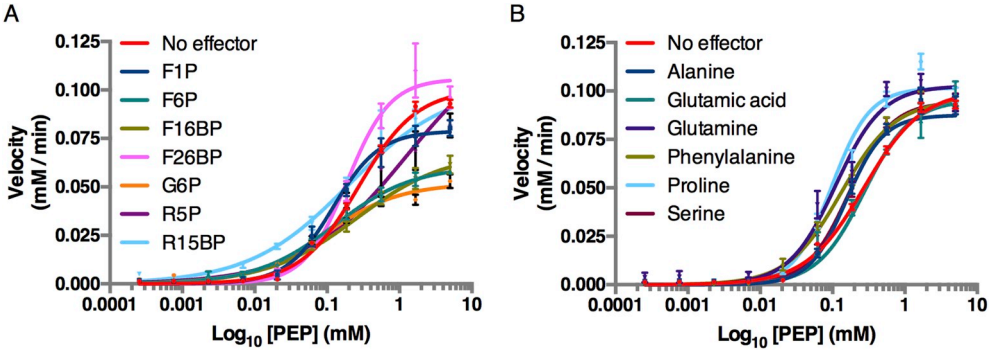

Fig. 1. AaPK1 enzymatic activity in the presence of effectors. (**A**) Phosphorylated sugars. (**B**) Amino acids. Derived kinetic constants are shown in Table 1. F1P = fructose-1-phosphate, F6P = fructose-6-phosphate, F16BP = fructose-1,6-bisphosphate, F26BP = fructose-2,6-bisphosphate, G6P = glucose-6-phosphate, R5P = ribulose-5-phosphate, R15BP = ribulose-1,5-bisphosphate. Data points represent means ± SEM of at least three replicates.

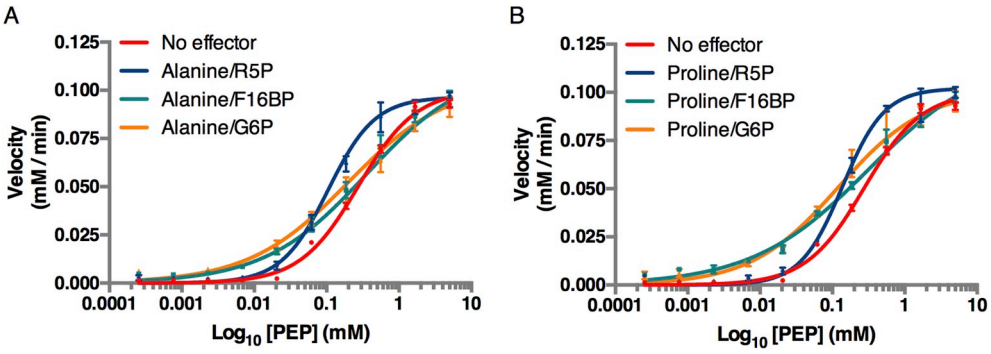

Fig. 2. AaPK1 enzymatic activity in the presence of sugars, alanine and proline. (**A**) Alanine and R5P/F16BP/G6P. (**B**) Proline and R5P/F16BP/G6P. Derived kinetic constants are shown in Table 1. R5P = ribulose-5-phosphate, F16BP = fructose-1,6-bisphosphate, G6P = glucose-6-phosphate. Data points represent means ± SEM of at least three replicates.

fold). Furthermore, the presence of these amino acids and sugar combinations raised the V_{max} by 12–20%, when compared to the control, and decreased the degree of cooperativity for PEP. Our data show that F16BP diminishes the enhanced effect of alanine, glutamine, proline, and serine on AaPK1 activity.

3.5. G6P alters the effect of alanine and serine on AaPK1 activity

We examined the influence of G6P in combination with alanine, glutamine, proline, or serine on AaPK1 kinetic parameters. We found that the addition of G6P to the reactions containing alanine significantly increased the K_{prime} (9-fold), when compared to alanine alone, and had no effect on the V_{max}. Similar results were found in the assays containing G6P and serine: 4- and 15-fold induction in the K_{prime} when compared to the control and serine alone, respectively, and no effect was observed on the V_{max}. On the other hand, the combination of glutamine and G6P did not affect the K_{prime} but decreased the V_{max} by 23%. However, when glutamine was replaced with proline, the K_{prime} and the V_{max} values of AaPK1 remained unchanged. Nevertheless, the combinations of G6P and each amino acid (alanine, proline, glutamine, or serine) weakened cooperativity for PEP binding (Table 1, Figs. 2 and 3). These results indicate that G6P reduces the effect of alanine and serine on AaPK1 activity.

3.6. Fluorescence thermal shift assays

The binding of the sugar and amino acid effectors was evaluated by changes in the melting temperature (T_m) of AaPK1. Changes are reported as the difference in melting temperatures (ΔT_m) between the protein in the presence of the effectors and the protein alone. Melting differences above 0.5 °C are considered indicative of binding (Mashalidis et al., 2013). Out of all the sugar and amino acid combinations that were tested, we only observed a significant increase in AaPK1 T_m in the presence of F16BP alone and in combination with the amino acids alanine, proline or serine (Table 2). The T_m recorded for the sugar-amino acid combinations was between 0.6 and 1 °C higher than the sugar alone, suggesting the presence of two effector binding sites. However, these amino acids did not increase the enzyme T_m by themselves, only in combination with F16BP. These results point to the interdependence of the two binding sites.

Table 2
Thermal shift assays.

Effector	ΔT_m (°C)
F16BP	3.33
Alanine/F16BP	4.00
Proline/F16BP	4.33
Serine/F16BP	4.33

Thermal shift assays were conducted using 0.125 μg/μl of AaPK1 in the absence and presence of 500 μM effector. F16BP = fructose-1,6-bisphosphate. Data are representative of 3 independent samples.

3.7. AaPK1 crystallization and structure description

Finally, we crystallized and determined the three-dimensional structure of AaPK1 bound to F16BP in the T-state. Several of the initial crystallization hits were optimized and large single protein crystals were obtained in the presence of different ligands, including allosteric compounds and enzyme substrates or products. These crystals did not diffract to high resolution despite significant efforts to optimize cryopreservation conditions. Therefore, we collected a 3.5 Å resolution data set from a crystal of AaPK1 bound to F16BP, and the 3D structure was solved by molecular replacement. The crystallographic statistics are listed in Table 3. The asymmetric unit cell included an AaPK1 tetramer, and the final model included all the residues with the exception of the initial ~20 residues for all chains (Fig. 4A). The AaPK1 showed an identical domain organization to enzymes from other organisms, a short N-terminal domain mostly missing from the electron density (Met1-Thr37), followed by the A central α/β barrel domain (Ala38-Gly114 and Ala218-Ala386). The β-strand B domain (Pro115-Pro217) protruded from the central domain, and a carboxy-terminus C domain

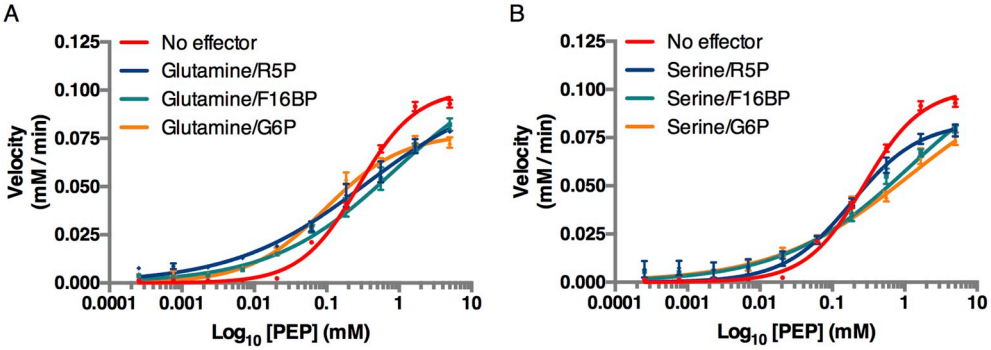

Fig. 3. AaPK1 enzymatic activity in the presence of sugars, glutamine and serine. (**A**) Glutamine and R5P/F16BP/G6P. (**B**) Serine and R5P/F16BP/G6P. Derived kinetic constants are shown in Table 1. R5P = ribulose-5-phosphate, F16BP = fructose-1,6-bisphosphate, G6P = glucose-6-phosphate. Data points represent means ± SEM of at least three replicates.

Table 3
Crystallographic statistics.

	AaPK1 F16BP	
Data collection		
Space group	$P2_12_12_1$	
Cell dimensions		
a, *b*, *c* (Å)	109.229 113.654 202.075	
α, β, γ (°)	90.00 90.00 90.00	
Resolution (Å)	49.530–3.51	3.72–3.51
R_{sym}	0.27	1.33
$I/\delta I$	5.8	1.0
Completeness (%)	99.8	99.5
Redundancy	3.9	3.8
Refinement		
Resolution (Å)	49.530–3.51	3.64–3.51
No. reflections	60460	5979
R_{work}/R_{free}	0.27/0.31	0.36/0.40
No. atoms		
Protein	15287	
Ligand/ion	84	
B-factors		
Protein	121.3	
Ligand/ion	94.5	
R.m.s. deviations		
Bond lengths (Å)	0.004	
Bond angles (°)	0.73	

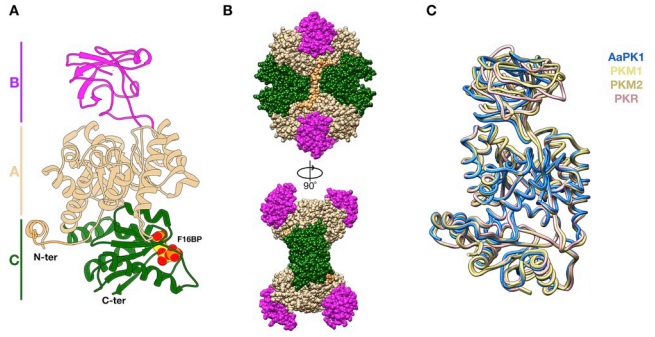

Fig. 4. AaPK1 crystallographic structure. (**A**) Cartoon representation of the AaPK1 monomer color-coded by domains, central A domain (tan), B domain (magenta) and C terminal domain (green). The effector F16BP is shown as spheres colored according to heteroatoms. (**B**) Two orthogonal views of the tetramer organization of AaPK1. (**C**) Overlay of AaPK1 (blue) with human enzymes, PKM1 (kaki), PKM2 (dark kaki) and PKR (pink).

(Leu387-Glu529) completed the monomer (Fig. 4A). The electron density quality was better in monomer I followed by monomers II, III and IV. The B domain electron density was well defined in monomer I, but poor electron density was observed in all other monomers. The PK enzyme was organized as a homotetramer, with two monomers interacting by their central A domains (2582 Å^2 average interacting surface), and then two dimers joined via their C domains (1084 Å^2 on average interacting surface) (Fig. 4B). The enzyme's active site was located in the cleft between domains A and B, and it was unoccupied in all monomers (despite the presence of oxaloacetate and ATP in the crystallization drop). Another component of the crystallization solution, F16BP, occupied all the C domain effector sites (Fig. 4A). Of the two allosteric sites, the effector site on the C domain and the amino acid site at the A-C domain interface, only the former were occupied by F16BP. A structural comparison of the AaPK1 with the previously determined PK from other organisms revealed that the mosquito enzyme shares a higher structural similarity with all the mammalian enzymes PKM1, PKM2 and PKR, with r.m.s.d. ≤1.7 Å^2 for rigid Cα atoms comparisons between monomers (Fig. 4C). Interestingly, higher sequence conservation did not account for higher structural similarities between mosquito and human PKs (Table 4 and Fig. 5). Finally, the quaternary structure of

Table 4
Sequence and structural similarity between AaPK1 and human PK isoforms.

	AaPK1	huPKM2	huPKM1	huPKR	huPKL
AaPK1		1.610	1.735	1.575	N/A
huPKM2	60.9/69.8		0.689	0.695	N/A
huPKM1	61.2/69.8	95.9/96.8		0.926	N/A
huPKR	57.1/68.2	71.4/80.6	70.1/79.1		N/A
huPKL	57.1/68.0	71.2/80.4	69.9/78.9	99.6/99.6	

Both sequence identity/similarity percentages are shown below the diagonal for all enzymes. The structural similarity is shown above the diagonal as rmsd (Å) for Cα superpositions (PDB ids: 3SRF huPKM1, 3SRD huPKM2, and 2VGB huPKR). The rmsd represents the average of four independent superpositions for each monomer.

AaPK1 was similar to the human PKR, PKM1 and PKM2 (R-state) structures, as evident by a superposition of a single monomer between the mosquito and human structures that produced an overlap of the tetramer. On the contrary, there was a significant divergence in the positions of the other monomers in the case of PKM2 in the T-state (Fig. S3).

4. Discussion

Mosquitoes typically emerge with teneral reserves that only assure limited flight performance and survival time. Immediately following eclosion, mosquitoes seek nectar for carbohydrates, and this is a common behavior for both male and female adult mosquitoes. Studies have shown that feeding on sugars increases survivorship in *A. aegypti* mosquitoes (Briegel et al., 2001; Foster, 1995). Carbohydrates are also required to support blood meal digestion, reproduction (Hou et al., 2015; Zhou et al., 2004), ammonia detoxification, and disposal of excess nitrogen in blood-fed *A. aegypti* females (Horvath et al., 2018), highlighting the importance of sugar metabolism in these insects. In this report, we demonstrate that the recombinant AaPK1 is allosterically regulated by specific sugars and amino acids.

The effect of phosphorylated sugars (both five- and six-carbon) on AaPK1 activity was first evaluated. Our results showed significant similarities at the amino acid sequence and structural levels between AaPK1 and the human non-allosteric isoform PKM1. This finding raised the possibility that allosteric compounds would not regulate the mosquito enzyme, or that AaPK would be affected by distinct phosphorylated sugars. The six-carbon sugar F1P was found to be a potent allosteric activator of AaPK1. Although F16BP is a major allosteric activator in most studied organisms that clearly binds to AaPK1, F1P has also been reported to regulate enzyme activity (Eggleston and Woods, 1970). Interestingly, the presence of the five-carbon sugar R5P decreased the affinity of AaPK1 to its substrate. It was previously demonstrated that R5P had no effect on *E. coli* PK kinetics when tested at concentrations up to 20 mM (Speranza et al., 1990). R5P is the final product of the oxidative phase of the pentose phosphate pathway (PPP), an alternative metabolic pathway for glucose oxidation. PPP is a major source of NADPH, which can be utilized in anabolic processes, used to protect cells from reactive oxygen species, and is required for the synthesis of nucleotide precursor ribose-5-phosphate. We recently demonstrated that glucose is partially metabolized through glycolysis and PPP during ammonia metabolism of blood-fed *A. aegypti* (Horvath et al., 2018). Here, we show allosteric inhibition of AaPK1 by R5P. The distinct inhibitory effect of R5P on AaPK1 activity suggests an additional mechanism for regulating PK activity in *A. aegypti* mosquitoes.

It was previously shown that the concentration of proline decreases, whereas the levels of alanine and glutamine increase, during flights of blood-fed *A. aegypti* females (Scaraffia and Wells, 2003). The amino acids proline, alanine, glutamine, glutamic acid and more recently serine have also been reported to be involved in ammonia detoxification in blood-fed *A. aegypti* females (Horvath et al., 2018; Isoe et al.,

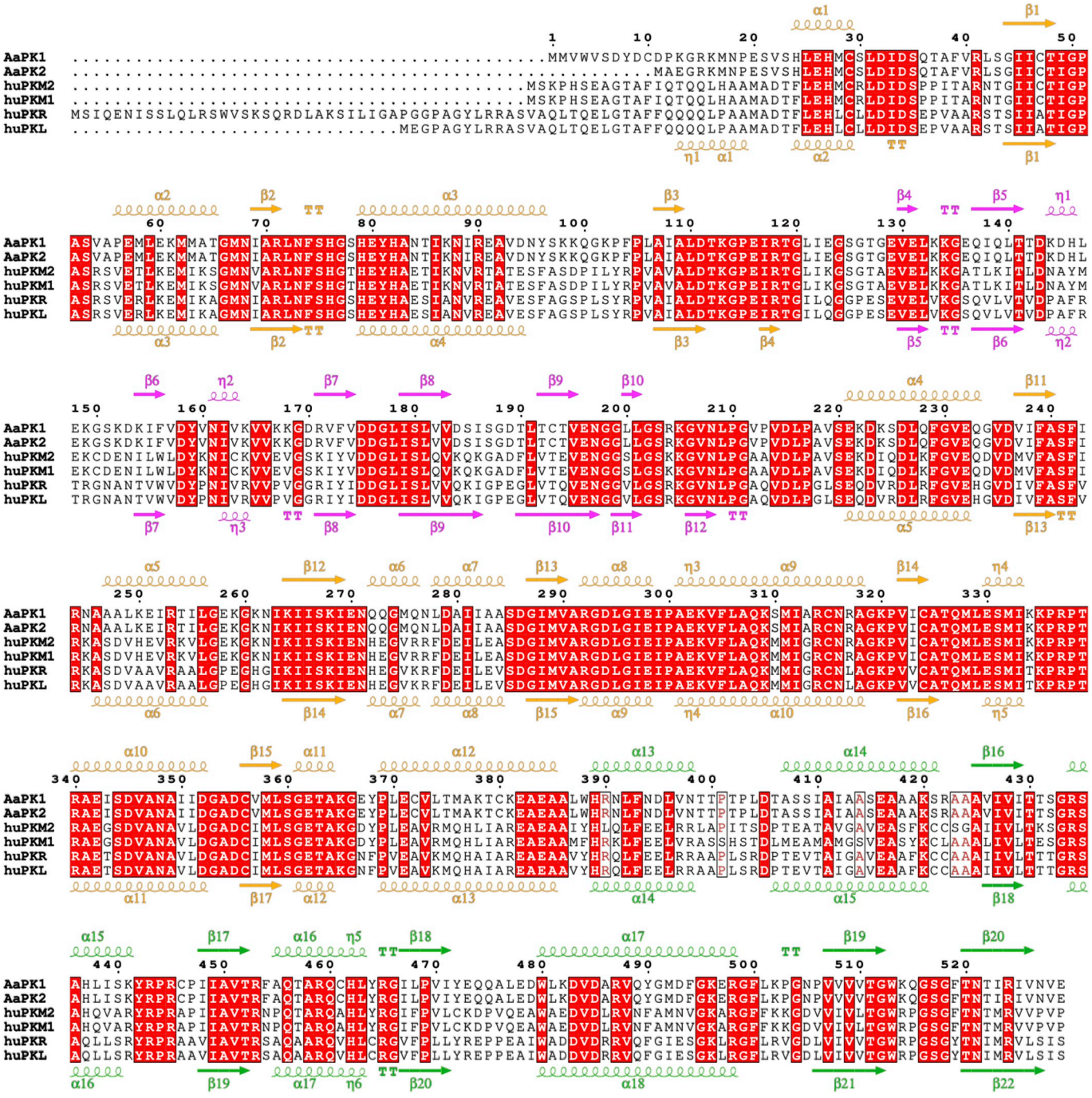

Fig. 5. *A. aegypti* and human PK isoforms multiple sequence alignment. AaPK1 and AaPK2 protein sequences are aligned to several human PK isoforms, huPKM1, huPKM2, huPKR and huPKL. The secondary elements of the AaPK1 structure are shown on top of the alignment and those of the huPKM1 structure (PDB id 3SRF) on the bottom. Secondary structure elements are color coded according to their domain: A domain (tan); B domain (magenta); and C domain (green).

2017; Mazzalupo et al., 2016; Scaraffia et al., 2005, 2006, 2008, 2010). Here, we found that alanine, glutamine, proline, and serine are allosteric activators of AaPK1. Moreover, in the presence of amino acids, the PK transcript level was reported to be upregulated in the fat body of *A. aegypti* (Hou et al., 2015). In addition, several studies have demonstrated that PK activity is regulated by a number of amino acids that can either enhance or inhibit its activity. In many organisms such as humans, rats, chickens, crickets and cockroaches, alanine and phenylalanine are allosteric inhibitors of PK (Hoffmann, 1975; Ibsen and Marles, 1976; Imamura and Tanaka, 1982; Llorente et al., 1970; Morgan et al., 2013; Storey, 1985; Van Berkel et al., 1973; Yuan et al., 2018). In *Trypanosoma brucei*, the enzyme is stimulated by phenylalanine, whereas alanine, glutamic acid, proline, and serine have no effect on the PK activity (Callens et al., 1991). In humans, serine functions as allosteric activator of PKM2 but not PKM1, PKL, and PKR (Chaneton et al., 2012; Yuan et al., 2018). The differential effect of amino acids on PK kinetic properties has also been reported in the three different isozymes of rat PK (Ibsen and Trippet, 1974). PK in the rat kidney cortex was strongly inhibited by alanine, phenylalanine and proline. However, the enzyme was activated by serine, whereas glutamine and glutamic acid had no effect on the enzyme activity. Likewise, the effect of the amino acids on the rat liver PK were similar to the rat kidney cortex enzyme except that serine was an allosteric inhibitor of the enzyme. For the rat muscle PK, phenylalanine was shown to be an inhibitor of the

enzyme and serine was an activator. Conversely, alanine, glutamine, glutamic acid, and proline had no effect on the rat muscle PK activity (Ibsen and Trippet, 1974). Recently, it was reported that in addition to phenylalanine and alanine, other amino acids (proline, tryptophan, methionine, valine, isoleucine and threonine) are inhibitors of human PKM2 (Yuan et al., 2018). Compared to other studied organisms, the results from our study show a unique pattern of AaPK regulation by amino acids.

Furthermore, we found that the presence of alanine, glutamine, proline or serine prevented the inhibitory effect of R5P on AaPK1. This implies that, under certain physiological conditions, these specific amino acids could increase glycolysis by activating AaPK1. We also showed that F16BP and G6P reduced the enhanced effect of amino acids on AaPK1 activity. When serine was added to the assay containing F16BP or G6P, the affinity of AaPK1 to its substrate was dramatically decreased. Interestingly, this counter effect of F16BP happens most probably with both effectors bound to the AaPK1 as shown by our fluorescence thermal shift assay results (Table 2). Serine is a precursor of several biosynthetic pathways. The synthesis of serine from the glycolytic intermediate, 3-phosphoglycerate could transiently reduce PK activity and the flux of carbon through glycolysis to facilitate uric acid synthesis and nitrogen waste disposal in blood-fed mosquitoes (Horvath et al., 2018).

Collectively, our data reveal how specific amino acids and phosphorylated sugars tightly regulate conformational dynamics and catalytic changes of AaPK1, thereby uncovering unique regulatory properties. Since nectar and host animal availability in nature may be unpredictable, the distinctive AaPK1 allosteric regulation could enable the rigorous metabolic control of carbon and nitrogen fluxes in sugar- and blood-fed mosquitoes, and therefore it could represent a critical regulatory point within mosquito metabolism.

Declarations of interest

The authors declare that they have no conflicts of interest with the contents of this article.

Funding information

Funding was provided by the Tulane University COR Research Fellowship, Corine Adams Professorship (to P.Y.S.), and Grant Number R01AI088092 from the National Institutes of Health (to P.Y.S.). The content is solely the responsibility of the authors and does not necessarily represent the official views of the National Institutes of Health.

Author contribution statement

J.C.P. and P.Y.S. conceived and designed experiments; N.P., C.M., J.I., and J.C.P. performed experiments; N.P., C.M., J.I., J.C.P., and P.Y.S. analyzed the data; N.P., J.C.P. and P.Y.S. wrote the manuscript.

Acknowledgments

X-ray diffraction data was collected at the Gulf Coast Protein Crystallography Consortium beamline at the Center for Advanced Microstructures and Devices, (CAMD – Baton Rouge, LA). The authors also thank Dr. H. D. Bellamy (CAMD-LSU) for assisting in data collection, and Dr. L. D. Brown for critical reading of the manuscript.

Appendix A. Supplementary data

Supplementary data to this article can be found online at https://doi.org/10.1016/j.ibmb.2018.12.010.

References

Adams, P.D., Afonine, P.V., Bunkóczi, G., Chen, V.B., Davis, I.W., Echols, N., Headd, J.J., Hung, L.W., Kapral, G.J., Grosse-Kunstleve, R.W., McCoy, A.J., Moriarty, N.W., Oeffner, R., Read, R.J., Richardson, D.C., Richardson, J.S., Terwilliger, T.C., Zwart, P.H., 2010. PHENIX: a comprehensive Python-based system for macromolecular structure solution. Acta Crystallogr. D Biol. Crystallogr. 66, 213–221. https://doi.org/10.1107/s0907444909052925.

Bailey, E., Walker, P.R., 1969. A comparison of the properties of the pyruvate kinases of the fat body and flight muscle of the adult male desert locust. Biochem. J. 111, 359–364. https://doi.org/10.1042/bj1110359.

Bakszt, R., Wernimont, A., Allali-Hassani, A., Mok, M.W., Hills, T., Hui, R., Pizarro, J.C., 2010. The crystal structure of *Toxoplasma gondii* pyruvate kinase 1. PLoS One 5, e12736. https://doi.org/10.1371/journal.pone.0012736.

Briegel, H., Knusel, I., Timmermann, S.E., 2001. *Aedes aegypti*: size, reserves, survival, and flight potential. J. Vector Ecol. 26, 21–31.

Callens, M., Kuntz, D.A., Opperdoes, F.R., 1991. Characterization of pyruvate kinase of *Trypanosoma brucei* and its role in the regulation of carbohydrate metabolism. Mol. Biochem. Parasitol. 47, 19–29. https://doi.org/10.1016/0166-6851(91)90144-U.

Chan, M., Sim, T.S., 2004. Functional analysis, overexpression, and kinetic characterization of pyruvate kinase from *Plasmodium falciparum*. Biochem. Biophys. Res. Commun. 326, 188–196. https://doi.org/10.1016/j.bbrc.2004.11.018.

Chaneton, B., Hillmann, P., Zheng, L., Martin, A.C., Maddocks, O.D., Chokkathukalam, A., Coyle, J.E., Jankevics, A., Holding, F.P., Vousden, K.H., Frezza, C., O'Reilly, M., Gottlieb, E., 2012. Serine is a natural ligand and allosteric activator of pyruvate kinase M2. Nature 491, 458–462. https://doi.org/10.1038/nature11540.

Collins, R.A., McNally, T., Fothergill-Gilmore, L.A., Muirhead, H., 1995. A subunit interface mutant of yeast pyruvate kinase requires the allosteric activator fructose 1,6-bisphosphate for activity. Biochem. J. 310, 117–123. https://doi.org/10.1042/bj3100117.

Copeland, R.A., 2000. Enzymes: A Practical Introduction to Structure, Mechanism, and Data Analysis, second ed.. Wiley-VCH, Inc., New York.

Eggleston, L.V., Woods, H.F., 1970. Activation of liver pyruvate kinase by fructose-1-phosphate. FEBS Lett. 6, 43–45. https://doi.org/10.1016/0014-5793(70)80038-2.

Emsley, P., Cowtan, K., 2004. Coot: model-building tools for molecular graphics. Acta Crystallogr. D Biol. Crystallogr. 60, 2126–2132. https://doi.org/10.1107/s0907444904019158.

Foster, W.A., 1995. Mosquito sugar feeding and reproductive energetics. Annu. Rev. Entomol. 40, 443–474. https://doi.org/10.1146/annurev.en.40.010195.002303.

Fothergill-Gillmore, L.A., Rigden, D.J., Michels, P.A., Phillips, S.E., 2000. *Leishmania* pyruvate kinase: the crystal structure reveals the structural basis of its unique regulatory properties. Biochem. Soc. Trans. 28, 186–190. https://doi.org/10.1042/bst0280186.

Gupta, R.K., Oesterling, R.M., Mildvan, A.S., 1976. Dual divalent cation requirement for activation of pyruvate kinase; essential roles of both enzyme- and nucleotide-bound metal ions. Biochemistry 15, 2881–2887. https://doi.org/10.1021/bi00658a028.

Hall, E.R., Cottam, G.L., 1978. Isozymes of pyruvate kinase in vertebrates: their physical, chemical, kinetic and immunological properties. Int. J. Biochem. 9, 785–793. https://doi.org/10.1016/0020-711X(78)90027-7.

Harrington, L.C., Edman, J.D., Scott, T.W., 2001. Why do female *Aedes aegypti* (Diptera: Culicidae) feed preferentially and frequently on human blood? J. Med. Entomol. 38, 411–422. https://doi.org/10.1603/0022-2585-38.3.411.

Harrington, L.C., Scott, T.W., Lerdthusnee, K., Coleman, R.C., Costero, A., Clark, G.G., Jones, J.J., Kitthawee, S., Kittayapong, P., Sithiprasasna, R., Edman, J.D., 2005. Dispersal of the dengue vector *Aedes aegypti* within and between rural communities. Am. J. Trop. Med. Hyg. 72, 209–220. https://doi.org/10.4269/ajtmh.2005.72.209.

Hoffmann, K., 1975. Pyruvate kinase from muscle and fat body of the house cricket *Acheta domesticus* L. : purification and catalytic studies. J. Comp. Physiol. 104, 59–69. https://doi.org/10.1007/BF02482837.

Horvath, T.D., Dagan, S., Lorenzi, P.L., Hawke, D.H., Scaraffia, P.Y., 2018. Positional stable isotope tracer analysis reveals carbon routes during ammonia metabolism of *Aedes aegypti* mosquitoes. Faseb. J. 32, 466–477. https://doi.org/10.1096/fj.201700657R.

Hou, Y., Wang, X.L., Saha, T.T., Roy, S., Zhao, B., Raikhel, A.S., Zou, Z., 2015. Temporal coordination of carbohydrate metabolism during mosquito reproduction. PLoS Genet. 11, e1005309. https://doi.org/10.1371/journal.pgen.1005309.

Ibsen, K.H., Marles, S.W., 1976. Inhibition of chicken pyruvate kinases by amino acids. Biochemistry 15, 1073–1079. https://doi.org/10.1021/bi00650a018.

Ibsen, K.H., Trippet, P., 1974. Effects of amino acids on the kinetic properties of three noninterconvertible rat pyruvate kinases. Arch. Biochem. Biophys. 163, 570–580. https://doi.org/10.1016/0003-9861(74)90516-5.

Iliffe-Lee, E.R., McClarty, G., 2002. Pyruvate kinase from *Chlamydia trachomatis* is activated by fructose-2,6-bisphosphate. Mol. Microbiol. 44, 819–828. https://doi.org/10.1046/j.1365-2958.2002.02924.x.

Imamura, K., Tanaka, T., 1982. Pyruvate kinase isozymes from rat. Methods Enzymol. 90, 150–165. https://doi.org/10.1016/S0076-6879(82)90121-5.

Isoe, J., Petchampai, N., Isoe, Y.E., Co, K., Mazzalupo, S., Scaraffia, P.Y., 2017. Xanthine dehydrogenase-1 silencing in *Aedes aegypti* mosquitoes promotes a blood feeding-induced adulticidal activity. Faseb. J. 31, 2276–2286. https://doi.org/10.1096/fj.201601185R.

Isoe, J., Scaraffia, P.Y., 2013. Urea synthesis and excretion in *Aedes aegypti* mosquitoes are regulated by a unique cross-talk mechanism. PLoS One 8, e65393. https://doi.org/10.1371/journal.pone.0065393.

Kabsch, W., 2014. Processing of X-ray snapshots from crystals in random orientations. Acta Crystallogr. D Biol. Crystallogr. 70, 2204–2216. https://doi.org/10.1107/

s1399004714013534.
Katzelnick, L.C., Coloma, J., Harris, E., 2017. Dengue: knowledge gaps, unmet needs, and research priorities. Lancet Infect. Dis. 17, e88–e100. https://doi.org/10.1016/s1473-3099(16)30473-x.
Kayne, F.J., 1973. Pyruvate kinase. In: third ed. In: Boyer, P.D. (Ed.), The Enzymes, vol. 8. Academic Press, NY, pp. 353–382. https://doi.org/10.1016/S1874-6047(08)60071-2.
Kwan, C.Y., Erhard, K., Davis, R.C., 1975. Spectral properties of Co(II)- and Ni(II)-activated rabbit muscle pyruvate kinase. J. Biol. Chem. 250, 5951–5959.
Llorente, P., Marco, R., Sols, A., 1970. Regulation of liver pyruvate kinase and the phosphoenolpyruvate crossroads. Eur. J. Biochem. 13, 45–54. https://doi.org/10.1111/j.1432-1033.1970.tb00897.x.
Lovell, S.C., Mullick, A.H., Muirhead, H., 1998. Cooperativity in *Bacillus stearothermophilus* pyruvate kinase. J. Mol. Biol. 276, 839–851. https://doi.org/10.1006/jmbi.1997.1569.
Mashalidis, E.H., Śledź, P., Lang, S., Abell, C., 2013. A three-stage biophysical screening cascade for fragment-based drug discovery. Nat. Protoc. 8, 2309–2324. https://doi.org/10.1038/nprot.2013.130.
Mattevi, A., Bolognesi, M., Valentini, G., 1996. The allosteric regulation of pyruvate kinase. FEBS Lett. 389, 15–19. https://doi.org/10.1016/0014-5793(96)00462-0.
Matthews, B.J., Dudchenko, O., Kingan, S.B., Koren, S., Antoshechkin, I., Crawford, J.E., Glassford, W.J., Herre, M., Redmond, S.N., Rose, N.H., Weedall, G.D., Wu, Y., Batra, S.S., Brito-Sierra, C.A., Buckingham, S.D., Campbell, C.L., Chan, S., Cox, E., Evans, B.R., Fansiri, T., Filipovic, I., Fontaine, A., Gloria-Soria, A., Hall, R., Joardar, V.S., Jones, A.K., Kay, R.G.G., Kodali, V.K., Lee, J., Lycett, G.J., Mitchell, S.N., Muehling, J., Murphy, M.R., Omer, A.D., Partridge, F.A., Peluso, P., Aiden, A.P., Ramasamy, V., Rasic, G., Roy, S., Saavedra-Rodriguez, K., Sharan, S., Sharma, A., Smith, M.L., Turner, J., Weakley, A.M., Zhao, Z., Akbari, O.S., Black, W.C.t., Cao, H., Darby, A.C., Hill, C.A., Johnston, J.S., Murphy, T.D., Raikhel, A.S., Sattelle, D.B., Sharakhov, I.V., White, B.J., Zhao, L., Aiden, E.L., Mann, R.S., Lambrechts, L., Powell, J.R., Sharakhova, M.V., Tu, Z., Robertson, H.M., McBride, C.S., Hastie, A.R., Korlach, J., Neafsey, D.E., Phillippy, A.M., Vosshall, L.B., 2018. Improved reference genome of *Aedes aegypti* informs arbovirus vector control. Nature 563, 501–507. https://doi.org/10.1038/s41586-018-0692-z.
Mazzalupo, S., Isoe, J., Belloni, V., Scaraffia, P.Y., 2016. Effective disposal of nitrogen waste in blood-fed *Aedes aegypti* mosquitoes requires alanine aminotransferase. Faseb. J. 30, 111–120. https://doi.org/10.1096/fj.15-277087.
McCoy, A.J., Grosse-Kunstleve, R.W., Adams, P.D., Winn, M.D., Storoni, L.C., Read, R.J., 2007. Phaser crystallographic software. J. Appl. Crystallogr. 40, 658–674. https://doi.org/10.1107/s0021889807021206.
Monath, T.P., Vasconcelos, P.F., 2015. Yellow fever. J. Clin. Virol. 64, 160–173. https://doi.org/10.1016/j.jcv.2014.08.030.
Morgan, H.P., McNae, I.W., Nowicki, M.W., Hannaert, V., Michels, P.A., Fothergill-Gilmore, L.A., Walkinshaw, M.D., 2010. Allosteric mechanism of pyruvate kinase from *Leishmania mexicana* uses a rock and lock model. J. Biol. Chem. 285, 12892–12898. https://doi.org/10.1074/jbc.M109.079905.
Morgan, H.P., O'Reilly, F.J., Wear, M.A., O'Neill, J.R., Fothergill-Gilmore, L.A., Hupp, T., Walkinshaw, M.D., 2013. M2 pyruvate kinase provides a mechanism for nutrient sensing and regulation of cell proliferation. Proc. Natl. Acad. Sci. U.S.A. 110, 5881–5886. https://doi.org/10.1073/pnas.1217157110.
Papadopoulos, A.I., Anagnostis, A., Lazarou, D., 2005. Effect of insecticide injection on pyruvate kinase of the insect *Tenebrio molitor* (Coleopteran). Pestic. Biochem. Physiol. 82, 115–124. https://doi.org/10.1016/j.pestbp.2005.01.002.
Russell, R.C., Webb, C.E., Williams, C.R., Ritchie, S.A., 2005. Mark-release-recapture study to measure dispersal of the mosquito *Aedes aegypti* in Cairns, Queensland, Australia. Med. Vet. Entomol. 19, 451–457. https://doi.org/10.1111/j.1365-2915.2005.00589.x.
Scaraffia, P.Y., Isoe, J., Murillo, A., Wells, M.A., 2005. Ammonia metabolism in *Aedes aegypti*. Insect Biochem. Mol. Biol. 35, 491–503. https://doi.org/10.1016/j.ibmb.2005.01.012.
Scaraffia, P.Y., Tan, G., Isoe, J., Wysocki, V.H., Wells, M.A., Miesfeld, R.L., 2008. Discovery of an alternate metabolic pathway for urea synthesis in adult *Aedes aegypti* mosquitoes. Proc. Natl. Acad. Sci. U.S.A. 105, 518–523. https://doi.org/10.1073/pnas.0708098105.
Scaraffia, P.Y., Wells, M.A., 2003. Proline can be utilized as an energy substrate during flight of *Aedes aegypti* females. J. Insect Physiol. 49, 591–601. https://doi.org/10.1016/S0022-1910(03)00031-3.
Scaraffia, P.Y., Zhang, Q., Thorson, K., Wysocki, V.H., Miesfeld, R.L., 2010. Differential ammonia metabolism in *Aedes aegypti* fat body and midgut tissues. J. Insect Physiol. 56, 1040–1049. https://doi.org/10.1016/j.jinsphys.2010.02.016.
Scaraffia, P.Y., Zhang, Q., Wysocki, V.H., Isoe, J., Wells, M.A., 2006. Analysis of whole body ammonia metabolism in *Aedes aegypti* using [^{15}N]-labeled compounds and mass spectrometry. Insect Biochem. Mol. Biol. 36, 614–622. https://doi.org/10.1016/j.ibmb.2006.05.003.
Speranza, M.L., Valentini, G., Malcovati, M., 1990. Fructose-1,6-bisphosphate-activated pyruvate kinase from *Escherichia coli*. Eur. J. Biochem. 191, 701–704. https://doi.org/10.1111/j.1432-1033.1990.tb19178.x.
Storey, K.B., 1985. Kinetic and regulatory properties of pyruvate kinase isozymes from flight muscle and fat body of the cockroach, *Periplaneta americana*. J. Comp. Physiol. B 155, 339–345. https://doi.org/10.1007/bf00687476.
Suzuki, K., Ito, S., Shimizu-Ibuka, A., Sakai, H., 2008. Crystal structure of pyruvate kinase from *Geobacillus stearothermophilus*. J. Biochem. 144, 305–312. https://doi.org/10.1093/jb/mvn069.
Van Berkel, T.J., Koster, J.F., Hulsmann, W.C., 1973. Some kinetic properties of the allosteric M-type pyruvate kinase from rat liver; influence of pH and the nature of amino acid inhibition. Biochim. Biophys. Acta 321, 171–180. https://doi.org/10.1016/0005-2744(73)90071-5.
Van Schaftingen, E., Opperdoes, F.R., Hers, H.G., 1985. Stimulation of *Trypanosoma brucei* pyruvate kinase by fructose 2,6-bisphosphate. Eur. J. Biochem. 153, 403–406. https://doi.org/10.1111/j.1432-1033.1985.tb09316.x.
Vital, W., Rezende, G.L., Abreu, L., Moraes, J., Lemos, F.J., Vaz Ida Jr., S., Logullo, C., 2010. Germ band retraction as a landmark in glucose metabolism during *Aedes aegypti* embryogenesis. BMC Dev. Biol. 10, 25. https://doi.org/10.1186/1471-213x-10-25.
Wang, C.K., Weeratunga, S.K., Pacheco, C.M., Hofmann, A., 2012. DMAN: a Java tool for analysis of multi-well differential scanning fluorimetry experiments. Bioinformatics 28, 439–440. https://doi.org/10.1093/bioinformatics/btr664.
Waygood, E.B., Rayman, M.K., Sanwal, B.D., 1975. The control of pyruvate kinases of *Escherichia coli*. II. Effectors and regulatory properties of the enzyme activated by ribose 5-phosphate. Can. J. Biochem. 53, 444–454. https://doi.org/10.1139/o75-061.
Wilder-Smith, A., Gubler, D.J., Weaver, S.C., Monath, T.P., Heymann, D.L., Scott, T.W., 2017. Epidemic arboviral diseases: priorities for research and public health. Lancet Infect. Dis. 17, e101–e106. https://doi.org/10.1016/s1473-3099(16)30518-7.
Yuan, M., McNae, I.W., Chen, Y., Blackburn, E.A., Wear, M.A., Michels, P.A.M., Fothergill-Gilmore, L.A., Hupp, T., Walkinshaw, M.D., 2018. An allostatic mechanism for M2 pyruvate kinase as an amino-acid sensor. Biochem. J. 475, 1821–1837. https://doi.org/10.1042/bcj20180171.
Yun, S.I., Lee, Y.M., 2017. Zika virus: An emerging flavivirus. J. Microbiol. 55, 204–219. https://doi.org/10.1007/s12275-017-7063-6.
Zhou, G., Flowers, M., Friedrich, K., Horton, J., Pennington, J., Wells, M.A., 2004. Metabolic fate of [^{14}C]-labeled meal protein amino acids in *Aedes aegypti* mosquitoes. J. Insect Physiol. 50, 337–349. https://doi.org/10.1016/j.jinsphys.2004.02.00.